

Constraints on accelerating universe using ESSENCE and Gold supernovae data combined with other cosmological probes

Jianbo Lu,* Lixin Xu, Molin Liu, and Yuanxing Gui

School of Physics and Optoelectronic Technology,

Dalian University of Technology, Dalian, 116024, P. R. China

We use recently observed data: the 192 ESSENCE type Ia supernovae (SNe Ia), the 182 Gold SNe Ia, the 3-year WMAP, the SDSS baryon acoustic peak, the X-ray gas mass fraction in clusters and the observational $H(z)$ data to constrain models of the accelerating universe. Combining the 192 ESSENCE data with the observational $H(z)$ data to constrain a parameterized deceleration parameter, we obtain the best fit values of transition redshift and current deceleration parameter $z_T = 0.632^{+0.256}_{-0.127}$, $q_0 = -0.788^{+0.182}_{-0.182}$. Furthermore, using Λ CDM model and two model-independent equation of state of dark energy, we find that the combined constraint from the 192 ESSENCE data and other four cosmological observations gives smaller values of Ω_{0m} and q_0 , but a larger value of z_T than the combined constraint from the 182 Gold data with other four observations. Finally, according to the Akaike information criterion it is shown that the recently observed data equally supports three dark energy models: Λ CDM, $w_{de}(z) = w_0$ and $w_{de}(z) = w_0 + w_1 \ln(1 + z)$.

PACS numbers: 98.80.-k

Keywords: deceleration parameter; equation of state (EOS); dark energy (DE); information criterion.

1. Introduction

The type Ia supernovae (SNe Ia) investigations [1], the cosmic microwave background(CMB) results from WMAP [2] observations, and surveys of galaxies [3] all suggest that the expansion of present universe is speeding up rather than slowing down. If one considers that the evolution of universe complies with the standard cosmology, the accelerated expansion of the present universe is usually attributed to the fact that dark energy (DE) is an exotic component with negative pressure. Many kinds of DE models have already been constructed such as Λ CDM [4], quintessence [5], phantom [6][7], generalized Chaplygin gas (GCG) [8][9], modified Chaplygin gas [10][11][12], quintom [13], holographic dark energy [14][15], agegraphic dark energy[16][17], and so forth.

On the other hand, to remove the dependence of special properties of extra energy components, a parameterized equation of state (EOS) is assumed for DE. This is also commonly called the model-independent method. The parameterized EOS of dark energy w_{de} which is popularly used in parameter best fit estimations, describes the possible evolution of DE. For example, $w_{de}(z) = w_0 = \text{const}$ [18], $w_{de}(z) = w_0 + w_1 \ln(1 + z)$ [19]. The parameters w_0 , w_1 are obtained by the best fit estimations from cosmic observational datasets.

Recently, the 192 ESSENCE SNe Ia data [20] was compiled by Ref. [21] using the four sets of supernova (SN)

*Electronic address: lvjianbo819@163.com

data: 60 ESSENCE SNe [22], 57 Supernova Legacy Survey (SNLS) SNe [23], 45 nearby SNe [1][24][25], and 30 new SNe at high redshift ($0.216 \leq z \leq 1.755$) recently discovered by the Hubble Space Telescope (HST) and classified as "Gold" SNe by Ref. [26]. The ESSENCE project [22] is a ground-based survey that design to detect about 200 SNe Ia in the range of $z = 0.2 - 0.8$ to measure the EOS of DE to better than 10 percent. The SNLS and the nearby SNe data as the complementary cosmological probes have been refitted by [22] with the same lightcurve fitter used for the ESSENCE data. As regards the 30 HST SNe, it is necessary to perform a normalization[27]. Ref. [21] adopted the low redshift SNe that these samples had in common in order to normalize the luminosity distances of the samples, and the error in the normalization is included in the distance errors for the HST SNe [21][27].

In Ref. [21] the authors applied the 192 ESSENCE SNe Ia data, the 3-year WMAP CMB shift parameter [28][29], the baryon acoustic oscillation (BAO) peak from Sloan Digital Sky Surver (SDSS) [30] to constrain the current values of EOS of DE w_{0de} and dimensionless matter density Ω_{0m} by using several model-independent EOS of DE. However, some other cosmological quantities such as transition redshift z_T and current deceleration parameter q_0 were not discussed. On the other hand, we know that the 182 Gold SNe Ia data [26] is compiled from five distinct subsets defined by the group or instrument that discovered and analyzed the corresponding SNe data. These subsets are [31][32]: the High z Supernova Search Team (HZSST) subset (41 SNe) [1][33][34][35], the Supernova Cosmology Project (SCP) subset (26 SNe) [36], the Low Redshift (LR) subset (38 SNe) [24][37][38][39], the HST subset (30 SNe) [26] and the SNLS subset (47 SNe) [23]. It can be found that there are 99 SNe that are in the 192 ESSENCE data but not in the 182 Gold data¹. Furthermore, relative to the Gold sample Ref. [21][22] applied an updated version of the MLCS2k2 method² to measure distances to SNe Ia for the ESSENCE sample, incorporating new procedures for K -correction and extinction corrections. So, the data points are also different even though for the same SNe in the two SN samples³. Therefore, we want to know what are the differences for the constraints on cosmological quantities from these two samples of SNe Ia respectively. In this paper, by using a parameterized deceleration parameter and model-independent EOS of DE, we apply the recent cosmic observations to constrain several cosmological quantities, such as z_T , q_0 , and compare the differences for them when the constraints are obtained from the 192 ESSENCE data and the 182 Gold data, respectively. To avoid the degeneration of DE models and get the significant constraints on cosmological quantities, we combine other observational data with these two sets of SNe data, such as the 3-year WMAP CMB shift parameter, the BAO peak from SDSS, the X-ray gas mass fraction in clusters [42] and the observational $H(z)$ data from the Gemini Deep Deep Survey (GDDS) [43] and archival data [44][45].

The paper is organized as follows. In section 2, we apply recent cosmic observations to constrain models of the accelerating universe by using a parameterized deceleration parameter q and model-independent EOS of DE w_{de} .

¹ The two sets of SNe Ia data with their subsets are shown in the Appendix. From the Appendix it can be seen that there are 93 SNe Ia in common between the 192 ESSENCE data and the 182 Gold data(i.e., from number 81 to number 173 in TABLE IV). They include 25 nearby SNe (or 25 LR SNe), 30 HST SNe and 38 SNLS SNe.

² The basic framework for Multicolor Light Curve Shape method to measure the luminosity distances was laid out by Ref. [38] in 2002 (i.e., MLCS2k2 method) and it has already been applied to SN Ia cosmology such as the 157 Gold SNe Ia data [40] and the 182 Gold SNe Ia data [26]. A new version of the MLCS2k2 was developed with an expanded training set by Ref. [25] and this light-curve fitting technique has also been applied to measure the luminosity distances to ESSENCE, SNLS and nearby SNe Ia in Ref. [22]. Because the basic MLCS2k2 algorithms were designed by Ref. [38], Refs. [22][25] continue to refer to this updated SN distance fitter as MLCS2k2, even though its implementation, applicability, and robustness have evolved substantially since then. For more details about MLCS2k2 please see Refs. [22][25][26][38][40][41].

³ For the case of the 192 ESSENCE data, since the error in the normalization is included in the distance errors for the HST SNe, the data points from the 30 HST SNe are also different between the 192 ESSENCE data and the 182 Gold data.

In section 3, we use the information criterion of model selection for DE models to estimate which model for an accelerating universe is distinguish by statistical analysis of observational datasets. Section 4 is the conclusion.

2. Constraining models of the accelerating universe

2.1 Constraining models of the accelerating universe using a parameterized deceleration parameter

The advantage of parameterizing $q(z)$ is that the conclusion does not depend on any particular gravitational theory [46]. In this section we consider a parameterized deceleration parameter $q(z) = \frac{1}{2} + \frac{a+bz}{(1+z)^2}$ [46][47], where a , b are constants. This deceleration parameter may have the same behavior as the simple three-epoch model [46]. Originally, the 157 Gold SNe Ia data was applied to constrain the transition redshift z_T by parameterizing a deceleration parameter $q(z) = q_0 + q_1 z$ in Ref. [40], and the result was given as $z_T = 0.46 \pm 0.13$ (1σ)⁴. However, it was soon realized that such a parametrization can not re-produce the behavior of the cosmological constant [48]. An alternative parametrization is a simple three-epoch model of $q(z)$ [49][50], where the function $q(z)$ is not smooth. Since the current SN Ia data is still sparse, the division of the data to three different redshift bins may not be a good representation of the data [46]. Then following Ref. [50], the authors in Ref. [46] proposed a simple smooth function $q(z) = \frac{1}{2} + \frac{a+bz}{(1+z)^2}$ which is more realistic and then used the 157 Gold SNe Ia data to constrain the z_T . In this paper using this parameterized deceleration parameter, we also want to know what are the best fit values of z_T and q_0 from the latest 192 ESSENCE SNe Ia data, and what are the differences for the constraints on z_T and q_0 when compare them with the constraint from Gold SNe Ia data. Next we will discuss these questions.

According to the definition of the Hubble parameter $H(t) = \frac{\dot{a}}{a}$ and the deceleration parameter $q(t) = -\frac{\ddot{a}}{aH^2}$, we get

$$H(z) = H_0 \exp\left[\int_0^z [1 + q(u)] d \ln(1 + u)\right]. \quad (1)$$

Substituting the expression $q(z) = \frac{1}{2} + \frac{a+bz}{(1+z)^2}$ into Eq. (1), we obtain

$$H^2(z) = H_0^2 E^2(z) = H_0^2 (1+z)^3 \exp\left[\frac{2az + (a+b)z^2}{(1+z)^2}\right]. \quad (2)$$

Since type Ia Supernovae behave as Excellent Standard Candles, they can be used to directly measure the expansion rate of the universe up to high redshift for comparison with the present rate. Therefore, they provide direct information on the universe's acceleration and constrain the DE model. Theoretical dark energy model parameters are determined by minimizing the quantity

$$\chi_{SNe}^2(H_0, \theta) = \sum_{i=1}^N \frac{(\mu_{obs}(z_i) - \mu_{th}(H_0, \theta, z_i))^2}{\sigma_{obs;i}^2}, \quad (3)$$

where $N = 192$ for the ESSENCE SNe Ia data [21], $\sigma_{obs;i}^2$ are errors due to flux uncertainties, intrinsic dispersion of SNe Ia absolute magnitude and peculiar velocity dispersion respectively. θ denotes model parameters. The theoretical distance modulus μ_{th} is defined as

$$\mu_{th}(z_i) \equiv m_{th}(z_i) - M = 5 \log_{10}(D_L(z)) + 5 \log_{10}\left(\frac{H_0^{-1}}{Mpc}\right) + 25, \quad (4)$$

⁴ In this paper, all errors are 1σ statistical errors.

where

$$D_L(z) = H_0 d_L(z) = (1+z) \int_0^z \frac{H_0 dz'}{H(z'; \theta)}, \quad (5)$$

μ_{obs} is given by supernovae dataset, and d_L is the luminosity distance. H is the Hubble parameter, "0" denotes the current value of the variable.

Thus on the basis of Eq. (2), we can use the maximum likelihood method for Eq. (3) to constrain parameters (H_0, a, b) . It should be noticed that, since we are interested in the model parameters a, b , the H_0 contained in $\chi_{SNe}^2(H_0, \theta)$ is a nuisance parameter and will be marginalized by integrating the likelihood $L(\theta) = \int dH_0 P(H_0) \exp(-\chi^2(H_0, \theta)/2)$. $P(H_0)$ is the prior distribution function of the current Hubble constant, and a Gaussian prior $H_0 = 72 \pm 8 km.S^{-1} Mpc^{-1}$ [51] is adopted in this paper. So, by using the maximum likelihood method to minimize the quantity χ_{SNe}^2 , we obtain the best fit model parameters $a = -1.287_{-0.387}^{+0.381}$, $b = -0.099_{-1.672}^{+1.727}$ with $\chi_{min}^2 = 195.495$. It can be seen that the number of degrees of freedom (dof) for this case is 190, here the value of dof of the model equals to the number of observational data points minus the number of parameters. Then the reduced χ^2 value (i.e., the ratio of the χ_{min}^2 value to the number of dof) is given as $\chi_{min}^2/dof = 1.029$. Furthermore, by fitting deceleration parameter $q(z) = \frac{1}{2} + \frac{a+bz}{(1+z)^2}$ to the 192 ESSENCE SNe Ia data, the 1σ error of the best fit $q(z)$ calculated by using the covariance matrix is plotted in FIG. 1(a). From FIG. 1(a), it can be seen that the evolution of q with respect to redshift z describes the current accelerating expansion of universe and the decelerating expansion in the past, and the best constraint on $q(z)$ from the 192 ESSENCE data lies in the redshift range $z \sim 0.2 - 0.4$. Also, we can see that the best fit values of transition redshift z_T and current deceleration parameter q_0 are $z_T = 0.644_{-0.194}^{+0.649}$, $q_0 = -0.787_{-0.253}^{+0.253}$. We compare these results with the ones obtained from Gold SNe Ia data. Considering Ref. [46], where $z_T = 0.36_{-0.08}^{+0.24}$ was obtained by using this deceleration parameter to the 157 Gold data, it is shown that the observations from 192 ESSENCE data tend to larger value of transition redshift. According to Ref. [52], where the model-independent method of using SNe Ia proposed and developed by Daly and Djorgovski [53][54] has been applied to constrain models of the accelerating universe from the 182 Gold SNe Ia data. The results were given as $z_T = 0.35_{-0.07}^{+0.15}$, $q_0 = -0.5_{-0.13}^{+0.13}$. We can see that this result of z_T (or q_0) is smaller (or larger) than the 192 ESSENCE case.

In order to get the more stringent constraints on transition redshift z_T and current deceleration parameter q_0 , we combine the 192 ESSENCE data with the observational $H(z)$ data. The Hubble parameter $H(z)$ depends on the differential age of the universe as a function of redshift z in the form

$$H(z) = -\frac{1}{1+z} \frac{dz}{dt}. \quad (6)$$

Therefore, the value of $H(z)$ can be directly measured through a determination of dz/dt . By using the differential ages of passively evolving galaxies from the GDDS [43] and archival data [44][45], Simon *et al.* obtained nine values of $H(z)$ in the range of $0 < z < 1.8$ [55]. Using these data we can constrain cosmological models by minimizing

$$\chi_{Hub}^2(H_0, \theta) = \sum_{i=1}^N \frac{[H_{th}(z_i) - H_{obs}(H_0, \theta, z_i)]^2}{\sigma_{obs;i}^2}, \quad (7)$$

where H_{th} is the predicted value for the Hubble parameter and can be given by Eq. (2), H_{obs} is the observed value, $\sigma_{obs;i}^2$ is the standard deviation measurement uncertainty. Here the nuisance parameter H_0 is marginalized. Then we combine two datasets to minimize the total likelihood χ_{total}^2

$$\chi_{total}^2(a, b) = \chi_{SNe}^2(a, b) + \chi_{Hub}^2(a, b). \quad (8)$$

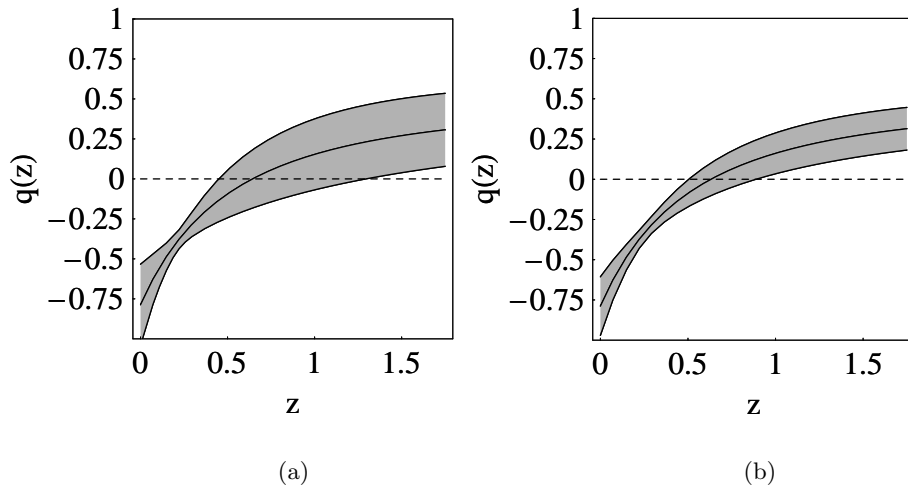


FIG. 1: The best fits of $q(z)$ with respect to redshift z constrained from the 192 ESSENCE SNe Ia data (a) and its combination with the 9 observational $H(z)$ data (b).

Case model	$H(z)$	$q(z)$
$w_{de}(z) = w_0 = \text{const}$	$H_0(1+z)^{\frac{3}{2}} [\Omega_{0m} + (1-\Omega_{0m})(1+z)^{3w_0}]^{\frac{1}{2}}$	$\frac{\Omega_{0m} + (1-\Omega_{0m})(1+3w_0)(1+z)^{3w_0}}{2[\Omega_{0m} + (1-\Omega_{0m})(1+z)^{3w_0}]}$
$w_{de}(z) = w_0 + w_1 \ln(1+z)$	$H_0(1+z)^{\frac{3}{2}} [\Omega_{0m} + (1-\Omega_{0m})(1+z)^{3(w_0+w_1)}]^{\frac{1}{2}}$	$\frac{\Omega_{0m} + (1-\Omega_{0m})(1+z)^{3(w_0+w_1z)} [1+3w_0+3w_1+(1+z)\ln(1+z)^{3w_1}]}{2[\Omega_{0m} + (1-\Omega_{0m})(1+z)^{3(w_0+w_1z)}]}$

TABLE I: The corresponding expressions of Hubble parameter $H(z)$ and deceleration parameter $q(z)$ for two w_{de}

By using the maximum likelihood method for Eq. (8), we obtain the best fit model parameters $a = -1.288^{+0.275}_{-0.276}$, $b = -0.068^{+1.010}_{-0.998}$ with $\chi^2_{min} = 205.254$. Here it can be seen that $\text{dof} = 199$, and $\chi^2_{min}/\text{dof} = 1.031$. The best fit evolution of $q(z)$ is plotted in FIG. 1(b) for combined constraint from the 192 ESSENCE data and the 9 observational $H(z)$ data. From Fig. 1(b) we can see that the best fit values of transition redshift z_T and current deceleration parameter q_0 are $z_T = 0.632^{+0.256}_{-0.127}$ and $q_0 = -0.788^{+0.182}_{-0.182}$. Replacing the 192 ESSENCE data with the 182 Gold data in the combined constraint, we find that the results for transition redshift and current deceleration parameter are $z_T = 0.502^{+0.180}_{-0.089}$, $q_0 = -0.692^{+0.202}_{-0.203}$. It is shown that the best fit value of z_T from the former combined constraint tends to larger value than the latter one. The central value of q_0 from the former combined constraint is smaller than the latter one. However, at 1σ error range the value of q_0 is almost consistent with being the same for the two combined constraints.

2.2 Constraining models of the accelerating universe using model-independent EOS of dark energy

Next we use the model-independent EOS of dark energy to constrain models of the accelerating universe and obtain the best fit values of z_T and q_0 . To obtain significant constraints on cosmological quantities, we combine other four cosmic observations: the 3-year WMAP CMB shift parameter, the SDSS baryon acoustic peak, the X-ray gas mass fraction in clusters, and the observational $H(z)$ data from the GDSS and archival data with the two samples of SNe Ia to constrain DE models. And we compare the differences for the constraints on cosmological quantities Ω_{0m} , w_{0de} , z_T and q_0 from the 192 ESSENCE data and the 182 Gold data with combining with other cosmic observations.

The structure of the anisotropies of the cosmic microwave background radiation depends on two eras in cosmology, i.e., last scattering and today. They can also be applied to limit the model parameters of DE by using the shift

parameter [56]

$$R = \sqrt{\Omega_{0m}} \int_0^{z_{rec}} \frac{H_0 dz'}{H(z'; \theta)}, \quad (9)$$

where $z_{rec} = 1089$ is the redshift of recombination. R obtained from the three-year WMAP data is [28]

$$R = 1.70 \pm 0.03. \quad (10)$$

From the CMB constraint, the best fit values of parameters in the DE models can be determined by minimizing

$$\chi_{CMB}^2(\theta) = \frac{(R(\theta) - 1.70)^2}{0.03^2}. \quad (11)$$

Because the universe has a fraction of baryons, the acoustic oscillations in the relativistic plasma would be imprinted onto the late-time power spectrum of the nonrelativistic matter [57]. Therefore, the acoustic signatures in the large-scale clustering of galaxies can also serve as a test to constrain models of DE with detection of a peak in the correlation function of luminous red galaxies in the SDSS [30]. By using the equation

$$A = \sqrt{\Omega_{0m}} E(z_{BAO})^{-1/3} \left[\frac{1}{z_{BAO}} \int_0^z \frac{dz'}{E(z'; \theta)} \right]^{2/3}, \quad (12)$$

and $A = 0.469 \pm 0.017$ measured from the SDSS data, $z_{BAO} = 0.35$, we can minimize the χ_{BAO}^2 defined as [58]

$$\chi_{BAO}^2(\theta) = \frac{(A(\theta) - 0.469)^2}{0.017^2}. \quad (13)$$

Where $E(z)$ is included in the Hubble parameter and can be given by defining $H(z) = H_0 E(z)$.

The observations of X-ray gas mass fraction in galaxy clusters provide key information on the dark matter, on the formation of structures in the universe, and can be used to constrain the cosmological parameters [59]. It is assumed that the baryon gas mass fraction in clusters [60]

$$f_{gas} = \frac{M_{b-gas}}{M_{tot}} \quad (14)$$

is constant, independent of redshift and is related to the global fraction of the universe Ω_b/Ω_{0m} . In the standard cold dark matter (SCDM) model, f_{gas}^{SCDM} is [60]

$$f_{gas}^{SCDM} = \frac{b}{1 + \alpha} \frac{\Omega_b}{\Omega_{0m}} \left(\frac{d_A^{SCDM}(z)}{d_A(z)} \right)^{\frac{3}{2}}, \quad (15)$$

where d_A is diameter distance which relates with d_L via $d_L(z) = (1+z)^2 d_A(z)$, the parameter b is a bias factor suggesting that the baryon fraction in clusters is slightly lower than for the universe as a whole, the parameter $\alpha \simeq 0.19\sqrt{h}$ is the ratio factor of optically luminous baryonic mass with X-ray gas contained in clusters. From Cluster Baryon Fraction (CBF), the best fit values of parameters in cosmological model can be determined by minimizing [60]

$$\chi_{CBF}^2(\theta) = C - \frac{B^2}{A}, \quad (16)$$

where

$$A = \sum_{i=1}^N \frac{\tilde{f}_{gas}^{SCDM}(z_i)^2}{\sigma_{f_{gas},i}^2},$$

Data	Case model	χ^2_{min}	χ^2_{min}/dof	Best fit model parameters
ESSENCE+R+A+ f_{gas} +H	Λ CDM	233.690	1.034	$\Omega_{0m} = 0.264^{+0.017}_{-0.017}$
	$w_{de}(z) = w_0 = \text{const}$	232.301	1.032	$\Omega_{0m} = 0.263^{+0.027}_{-0.024}, w_0 = -0.996^{+0.106}_{-0.116}$
Gold+R+A+ f_{gas} +H	$w_{de}(z) = w_0 + w_1 \ln(1+z)$	231.106	1.032	$\Omega_{0m} = 0.272^{+0.027}_{-0.024}, w_0 = -1.041^{+0.127}_{-0.142}, w_1 = 0.003^{+0.003}_{-0.084}$
	Λ CDM	200.355	0.928	$\Omega_{0m} = 0.280^{+0.019}_{-0.017}$
	$w_{de}(z) = w_0 = \text{const}$	197.356	0.918	$\Omega_{0m} = 0.280^{+0.028}_{-0.027}, w_0 = -0.899^{+0.110}_{-0.122}$
	$w_{de}(z) = w_0 + w_1 \ln(1+z)$	196.651	0.918	$\Omega_{0m} = 0.287^{+0.028}_{-0.027}, w_0 = -0.939^{+0.130}_{-0.149}, w_1 = 0.002^{+0.003}_{-0.087}$

TABLE II: The values of χ^2_{min} , χ^2_{min}/dof , and best fit model parameters against the model

Data	Case model	z_T	q_0
ESSENCE+R+A+ f_{gas} +H	Λ CDM	$0.774^{+0.051}_{-0.050}$	$-0.605^{+0.025}_{-0.025}$
	$w_{de}(z) = w_0 = \text{const}$	$0.776^{+0.055}_{-0.053}$	$-0.600^{+0.082}_{-0.083}$
	$w_{de}(z) = w_0 + w_1 \ln(1+z)$	$0.742^{+0.062}_{-0.056}$	$-0.637^{+0.091}_{-0.090}$
Gold +R+A+ f_{gas} +H	Λ CDM	$0.725^{+0.051}_{-0.051}$	$-0.579^{+0.026}_{-0.027}$
	$w_{de}(z) = w_0 = \text{const}$	$0.728^{+0.059}_{-0.061}$	$-0.471^{+0.088}_{-0.088}$
	$w_{de}(z) = w_0 + w_1 \ln(1+z)$	$0.706^{+0.063}_{-0.060}$	$-0.504^{+0.097}_{-0.098}$

TABLE III: The best fit values of transition redshift z_T and current deceleration parameter q_0 against the model

$$B = \sum_{i=1}^N \frac{\tilde{f}_{gas}^{SCDM}(z_i) \cdot f_{gas,i}}{\sigma_{f_{gas,i}}^2},$$

$$C = \sum_{i=1}^N \frac{f_{gas,i}^2}{\sigma_{f_{gas,i}}^2}, \quad (17)$$

and

$$\tilde{f}_{gas}^{SCDM}(z_i) = \left(\frac{d_A^{SCDM}(z)}{d_A(z)} \right)^{\frac{3}{2}}. \quad (18)$$

$N = 26$ is the number of the observed $f_{gas,i}$ and $\sigma_{gas,i}^2$ published in Ref. [42].

Next, using the datasets of above observational techniques, we minimize the total likelihood χ^2_{total} [61]

$$\chi^2_{total} = \chi^2_{SNe} + \chi^2_{Hub} + \chi^2_{CMB} + \chi^2_{BAO} + \chi^2_{CBF}. \quad (19)$$

In this paper we consider two combined constraints on DE models from recently observed data, i.e., the 192 ESSENCE SNe Ia data and the 182 Gold SNe Ia data are combined with other four observational datasets, respectively. χ^2_{total} for these two cases can be written as $\chi^2_{total1} = \chi^2_{192SNe} + \chi^2_{Hub} + \chi^2_{CMB} + \chi^2_{BAO} + \chi^2_{CBF}$, and $\chi^2_{total2} = \chi^2_{182SNe} + \chi^2_{Hub} + \chi^2_{CMB} + \chi^2_{BAO} + \chi^2_{CBF}$. For simplicity, we express the cosmic observations as 192 ESSENCE+Hub+CMB+BAO+CBF and 182 Gold+Hub+CMB+BAO+CBF for the two combined constraints in the following part.

Here we consider two model-independent EOS of DE, $w_{de}(z) = w_0 = \text{const}$ [18] (one-parameter model) and $w_{de}(z) = w_0 + w_1 \ln(1+z)$ [19] (two-parameter model). For a flat universe, the corresponding Hubble parameter $H(z)$ and deceleration parameter $q(z)$ are derived and listed in TABLE I for these two $w_{de}(z)$. Besides, we also consider

the most popular model Λ CDM. The Hubble parameter $H(z)$ and deceleration parameter $q(z)$ for this model can be obtained from TABLE I when $w_0 = -1$ for the case of $w_{de}(z) = w_0$.

Thus on the basis of the expressions of $H(z)$ and $q(z)$ in TABLE I, we can obtain the best fit parameters against the model with its χ^2_{min} value by using the maximum likelihood method for Eq. (19). Furthermore, the reduced χ^2 can also be calculated against the model. TABLE II lists the results. From TABLE II we can see that the central value of current dimensionless matter density Ω_{0m} is about $0.26 \sim 0.27$ for the constraint from 192 ESSENCE+Hub+CMB+BAO+CBF. Comparing with the combined constraint from 182 Gold+Hub+CMB+BAO+CBF, it means the former combined constraint tends to smaller current value of matter density Ω_{0m} than the latter one, where the central value of Ω_{0m} is about $0.28 \sim 0.29$ for these three DE models. In addition, it is shown that for DE model $w_{de}(z) = w_0 + w_1 \ln(1+z)$, the best fit value of model parameter w_1 has small value for the both combined constraints. It may be said that the model $w_{de}(z) = w_0 + w_1 \ln(1+z)$ has a small correctional function relative to the case of $w_{de}(z) = w_0 = \text{const}$. At last, it can be seen that for the case of $w_{de}(z) = w_0 = \text{const}$, the central value of current EOS of DE w_{0de} is surprisingly close to Λ CDM model ($w_{de}(z) = -1$) for the constraint from 192 ESSENCE+Hub+CMB+BAO+CBF.

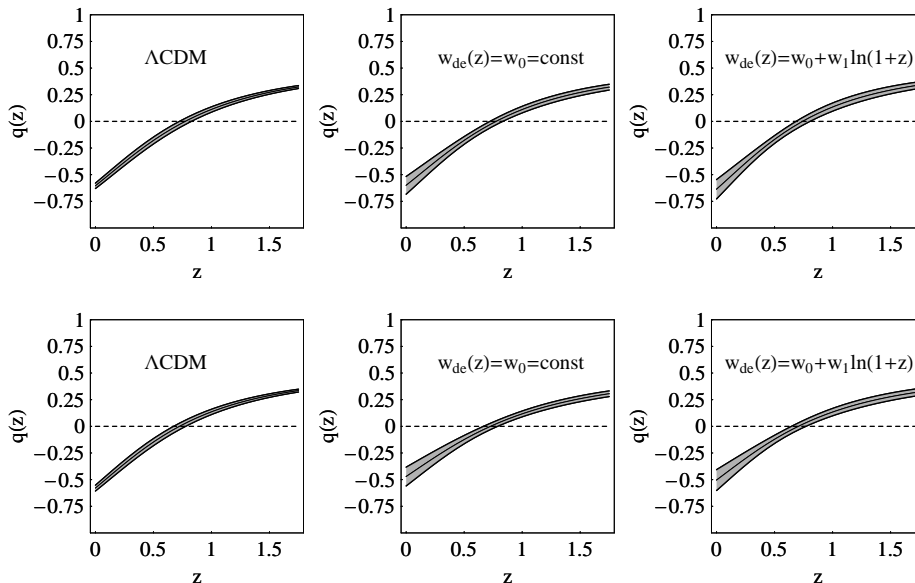


FIG. 2: The best fits of $q(z)$ with 1σ error for three dark energy models constrained from 192 ESSENCE+Hub+CMB+BAO+CBF (upper) and 182 Gold+Hub+CMB+BAO+CBF (lower), respectively.

FIG.2 shows the 1σ error of the best fit $q(z)$ calculated by using the covariance matrix for three DE models. From FIG.2 we can get the best fit values of transition redshift z_T and current deceleration parameter q_0 against the model from two combined constraints. The results are listed in TABLE III. We know that transition redshift z_T denotes the time when the evolution of universe changes from decelerated expansion to accelerated expansion. The larger value of z_T , the earlier time of turning into an accelerating universe. The value of q_0 indicates the expansion rhythm of present universe. The smaller value of q_0 , the more violent of universe's acceleration. From TABLE III, it can be found that, though at 1σ error range the differences between the two combined constraints for the values of z_T and q_0 are not very obvious, the central values of z_T constrained from 192 ESSENCE+Hub+CMB+BAO+CBF are

Case model	AIC	ΔAIC_i	$w_{i(AIC)}$	BIC	ΔBIC_i	$w_{i(BIC)}$
Λ CDM	235.690	0	0.449	239.115	0	0.712
$w_{de}(z) = w_0 = \text{constant}$	236.301	0.611	0.330	243.151	4.036	0.257
$w_{de}(z) = w_0 + w_1 \ln(1+z)$	237.106	1.416	0.221	247.381	8.266	0.031

TABLE IV: The values of AIC, AIC difference, AIC weight, BIC, BIC difference and BIC weight against the model for the constraint form 192 ESSENCE+Hub+CMB+BAO+CBF

Case model	AIC	ΔAIC_i	$w_{i(AIC)}$	BIC	ΔBIC_i	$w_{i(BIC)}$
Λ CDM	202.355	0.999	0.285	205.735	0	0.525
$w_{de}(z) = w_0 = \text{constant}$	201.356	0	0.469	208.116	2.381	0.434
$w_{de}(z) = w_0 + w_1 \ln(1+z)$	202.651	1.295	0.246	212.791	7.056	0.041

TABLE V: The values of AIC, AIC difference, AIC weight, BIC, BIC difference and BIC weight against the model for the constraint form 182 Gold+Hub+CMB+BAO+CBF

bigger than the cases of 182 Gold+Hub+CMB+BAO+CBF, and the central values of q_0 are smaller than the cases of 182 Gold SNe Ia+Hub+CMB+BAO+CBF. Furthermore, we can see that the cosmic acceleration could have started between the redshift $z_T = 0.706^{+0.063}_{-0.060}$ and $z_T = 0.774^{+0.051}_{-0.050}$ for these two combined constraints.

3. Model selection and Information criterion

Since the emphasis of the ongoing and forthcoming research is shifting from estimating specific parameters of the cosmological model to model selection [62], it is interesting to estimate which model for an accelerating universe is distinguish by statistical analysis of observational datasets out of a large number of cosmological models. A popular but not too refined method to rate goodness of models is to compare the quantity χ^2_{min}/dof [27]. From TABLE II we can see that, both the 192 ESSENCE and the 182 Gold data cases show a slightly higher χ^2_{min}/dof for the Λ CDM model, i.e., the Λ CDM model has a less support from recent observations when compare it with other two DE models. In this paper we also use the objective model selection criteria, including the Akaike information criterion (AIC) and the Bayesian information criterion (BIC), to estimate the strength of models.

In cosmology the information criterion (IC) was first used by Liddle [63], and then in subsequent papers [65][66]. The AIC was derived by Akaike, and it takes the form

$$AIC = -2 \ln \mathcal{L}(\theta | data)_{\max} + 2K, \quad (20)$$

where \mathcal{L}_{max} is the highest likelihood in the model with the best fit parameters θ , K is the number of estimable parameters (θ) in the model. The term $-2 \ln \mathcal{L}(\theta | data)$ in Eq. (20) is called χ^2 and it measures the quality of model fit, while the term $2K$ in Eq. (20) interprets model complexity. The BIC is similar to the AIC, but the second term is different. It was derived by Schwarz and is written as

$$BIC = -2 \ln \mathcal{L}(\theta | data)_{\max} + K \ln n, \quad (21)$$

where n is the number of data points in the datasets.

Now the question is how to assess the strength of models. We take the AIC case as an example. The value of AIC has no meaning by itself for a single model and only the relative value between different models are physically interesting. Therefore, by comparing several models the one which minimizes the AIC is usually considered the best, and denoted by $AIC_{min} = \min\{AIC_i, i = 1, \dots, N\}$, where $i = 1, \dots, N$ is a set of alternative candidate models. The relative strength of evidence for each model can be obtained by calculating the relative likelihood of the model $\mathcal{L}(M_i | data) \propto \exp(-\Delta AIC_i/2)$, where $\Delta AIC_i = AIC_i - AIC_{min}$ over the whole range of alternative models. The Akaike weights $w_{i(AIC)}$ are calculated by normalizing the relative likelihoods of the models $\mathcal{L}(M_i | data)$ to unity. The rules for judging the AIC model selection are as follows [62]: when $0 \leq \Delta AIC_i \leq 2$ model i has almost the same support from the data as the best model, for $2 \leq \Delta AIC_i \leq 4$, model i is supported considerably less and with $\Delta AIC_i > 10$ model i is practically irrelevant. According to Eq. (20) we can get the BIC values of several models. The model that have the minimum BIC value is considered the best. Then similar to the AIC case, taking it as a reference, the BIC difference and BIC weight against the model can be calculated. The rules for judging the BIC model selection are described as [21][63]: a ΔBIC of more than 2 (or 6) relative to the best one is considered "unsupported" (or "strongly unsupported") from observational data. Furthermore, it should be noticed that according to Ref. [64], in the limit of large data points (large n) AIC tends to favor models with more parameters while BIC tends to penalize them. For more details about AIC and BIC, please see Refs. [62][63][64][65][66][67][68].

In what follows, we will estimate which model is the best-fit one according to the AIC and BIC for all the models in Table II. Based on the values of χ^2_{min} , it is shown that the best model is the one following Λ CDM in terms of its AIC value for the constraint from 192 ESSENCE+Hub+CMB+BAO+CBF, and the best one is $w_{de}(z) = w_0$ for the constraint from 182 Gold+Hub+CMB+BAO+CBF. For the case of each combined constraint, taking its minimum AIC value as a reference, we obtain the AIC differences ΔAIC_i , Akaike weights $w_{i(AIC)}$ against alternative models. TABLE IV and V list the calculating results for the cases of two combined constraints. Note that the model selection provides quantitative information to judge the "strength of evidence", not just a way to select only one model. From TABLE IV and V, it can be seen that three DE models have almost the same support from two datasets because the values of ΔAIC_i for other two models are in the range 0-2 relative to the best one. The calculation for the BIC is similar to the AIC case, and the results are listed in TABLE IV and V, too. In this analysis, we find the best fit model is Λ CDM for the both combined constraints, and the more free parameters in DE model, the weaker support from observational data for these three DE models.

According to the AIC we can see that the model degeneration is obvious because three DE models have almost the same support from observational data. Then we expect the new probers such as SNAP and Planck surveyor can provide more accurate data and break up the model degeneration. For the BIC, it is shown that this model selection method can be a better one to avoid the model degeneration than the AIC.

4. Conclusion

In summary, we use the 192 ESSENCE SNe Ia data and the 182 Gold SNe Ia data combined with other observed data such as the 3-year WMAP, the BAO peak from SDSS, the X-ray gas mass fraction in clusters and the observational $H(z)$ data from the GDDS and archival data, to constrain models of the accelerating universe. Concretely, using the 192 ESSENCE SNe Ia data and the 9 observational $H(z)$ data to constrain a parameterized

deceleration parameter $q(z) = \frac{1}{2} + \frac{a+bz}{(1+z)^2}$ [46][47], we obtain the best fit model parameters, $a = -1.288_{-0.276}^{+0.275}$, $b = -0.068_{-0.998}^{+1.010}$. The best fit values of transition redshift z_T and current deceleration parameter q_0 are given as $z_T = 0.632_{-0.127}^{+0.256}$, $q_0 = -0.788_{-0.182}^{+0.182}$. Replacing the 192 ESSENCE data with the 182 Gold data in combined constraint, it can be found that at 1σ error range, this result for q_0 is almost consistent with being the same for the two combined constraints. But the result for z_T at 1σ error range tends to larger value than the case of the joint analysis involving the 182 Gold data and the observational $H(z)$ data. Furthermore, it is shown that the central value of z_T (or q_0) for the former combined constraint is larger (or smaller) than latter one. For producing the differences of these cosmological quantities between these two combined constraints, the reason maybe is caused by the different way that the SNe magnitudes are calculated for the two samples of SNe Ia. On the other hand, since some data points in the two sets of SN data are from the different subsets, some unknown system errors from the different instruments for SNe surveys are also possible to contribute to these differences for the cosmological quantities. We also expect the more advanced probes to explore SNe in future.

Furthermore, for the cosmological quantities Ω_{0m} , w_{0de} , z_T and q_0 , we compare the differences for them between the combined constraint from the 192 ESSENCE data with other four cosmic observations and the 182 Gold data with other four observations. Considering DE model Λ CDM and two model-independent EOS of dark energy, $w_{de}(z) = w_0$, $w_{de}(z) = w_0 + w_1 \ln(1+z)$, we plot the best fit forms of deceleration parameter $q(z)$ with 1σ error by using two sets of SNe data with other cosmological observations. It can be seen that the cosmic acceleration could have started between the redshift $z_T = 0.706_{-0.060}^{+0.063}$ and $z_T = 0.774_{-0.050}^{+0.051}$ for two combined constraints. By comparing the two combined constraints on the DE models: Λ CDM, $w_{de}(z) = w_0$, and $w_{de}(z) = w_0 + w_1 \ln(1+z)$, we find that the combined constraint from 192 ESSENCE+Hub+CMB+BAO+CBF tends to smaller current value of matter density Ω_{0m} than the constraint from 182 Gold+Hub+CMB+BAO+CBF. And it can be seen that, though at 1σ error range the differences between two combined constraints for the values of z_T and q_0 are not very obvious, the central values of z_T constrained from 192 ESSENCE+Hub+CMB+BAO+CBF are bigger than the cases of 182 Gold+Hub+CMB+BAO+CBF, and the central values of q_0 are smaller than the cases of 182 Gold SNe Ia+Hub+CMB+BAO+CBF. At last, it is shown that for the case of $w_{de}(z) = w_0 = \text{const}$, the central value of w_{0de} constrained from 192 ESSENCE+Hub+CMB+BAO+CBF is surprisingly close to Λ CDM model ($w_{de} = -1$).

Since it is interesting to estimate which model for an accelerating universe is distinguish by statistical analysis of observational datasets over many models, by applying the recent observational data to the objective information criterion of model selection, we compare with three DE models in TABLE II to assess the strength of models. It is shown that, according to the AIC though the best model is Λ CDM for using the combined datasets of 192 ESSENCE+Hub+CMB+BAO+CBF, other two models also have the same support with the best one because the values of ΔAIC_i for them are in the range 0-2. For the case of the BIC we find the best fit model is Λ CDM for both combined constraints, and the more free parameters in DE model, the weaker support from observational data for these three DE models.

Acknowledgments The research work is supported by NSF (10573003), NSF (10573004), NSF (10703001), and

NSF (10647110), NBRP (2003CB716300) of P.R. China.

- [1] A.G. Riess et al., *Astron. J.* **116**, 1009 (1998) [astro-ph/9805201]
- [2] D.N. Spergel, et. al, *Astrophys. J. Suppl.* **148**, 175 (2003) [astro-ph/0302209]
- [3] A.C. Pope, et. al, *Astrophys. J.* **607**, 655 (2004) [astro-ph/0401249]
- [4] S. Weinberg, *Mod. Phys. Rev.* **61**, 527 (1989)
- [5] B. Ratra, P.J.E. Peebels, *Phys. Rev. D.* **37**, 3406 (1988)
- [6] R.R. Caldwell, M. Kamionkowski, N. N. Weinberg, *Phys. Rev. Lett.* **91**, 071301 (2003) [astro-ph/0302506]
- [7] M.R. Setare, *Eur. Phys. J. C* **50**, 991 (2007)
- [8] A.Y. Kamenshchik, U. Moschella, V. Pasquier, *Phys. Lett. B* **511**, 265 (2001) [gr-qc/0103004]
- [9] H.S Zhang, Z.H. Zhu , *Phys. Rev. D* **73**, 043518 (2006) [arXiv:astro-ph/0509895]
- [10] H.B. Benaoum, [hep-th/0205140]
- [11] J.B. Lu, L.X. Xu, J.C. Li, B.R. Chang, Y.X. Gui, H.Y. Liu, *Phys. Lett. B* **662**, 87 (2008)
- [12] J.B. Lu, L.X. Xu, J.C. Li, H.Y. Liu,, *Mod. Phys. Lett. A* **23**, 25 (2008)
- [13] B. Feng, X.L. Wang, X.M. Zhang, *Phys. Lett. B* **607**, 35 (2005) [astro-ph/0404224]
- [14] M. Li, *Phys. Lett. B* **603**, 1 (2004) [hep-th/0403127]
- [15] J.F. Zhang, X. Zhang, H.Y. Liu, *Eur. Phys. J. C* **52**, 693 (2007)
- [16] R.G. Cai, *Phys. Lett. B* 657, 228 (2007) [arXiv:hep-th/ 0707.4049]
- [17] J.F. Zhang, X. Zhang, H.Y. Liu, *Eur. Phys. J. C* **54**, 303 (2008)
- [18] S. Hannestad, E. Mortsell, *Phys. Rev. D* **66**, 063508 (2002)
- [19] B.F. Gerke, G. Efstathiou, *Mon. Not. Roy. Astron. Soc.* **335**, 33 (2002) [astro-ph/0201336]
- [20] Q. Wu, Y.G. Gong, A.Z. Wang, J.S. Alcanizd, *Phys. Lett. B* **659**, 34 (2008)
- [21] T.M. Davis et al., [astro-ph/0701510]; also <http://www.dark-cosmology.dk/archive/SN> or <http://braeburn.pha.jhu.edu/~ariess/R06> or <http://www.ctio.noao.edu/essence>
- [22] W.M. Wood-Vasey et al., [astro-ph/0701041]
- [23] P. Astier et al., *Astron. Astrophys.* **447**, 31 (2006) [arXiv:astro-ph/0510447]
- [24] M. Hamuy, M. M. Phillips, N. B. Suntzeff, R. A. Schommer, J. Maza, *Astron. J.* **112** 2408 (1996) [arXiv:astro-ph/9609064]
- [25] S. Jha, A. G. Riess, R. P. Kirshner, *Astrophys. J.* **659**, 122 (2007) [arXiv:astro-ph/0612666]
- [26] A.G. Riess et al., [astro-ph/0611572]
- [27] R. Lazkoz, E. Majerotto, [arXiv:0704.2606]
- [28] D.N. Spergel et al., *Astrophys. J. Suppl.* **170**, 377 (2007) [astro-ph/0603449]
- [29] Y. Wang, P. Mukherjee, *Astrophys. J.* **650**, 1 (2006) [astro-ph/0604051]
- [30] D.J. Eisenstein et al., *Astrophys. J.* **633**, 560 (2005) [astro-ph/0501171]
- [31] S. Nesseris and L. Perivolaropoulos, *J. Cosmol. Astron. Phys.* **0702** 025 (2007), astro-ph/0612653
- [32] <http://www.tass-survey.org/richmond/sne/sn.list>
- [33] B.F. Williams et al., [astro-ph/0310432]
- [34] A.G. Riess et al., *Astrophys. J.* **536** 62 (2000) [astro-ph/0001384]
- [35] J.L. Tonry et al., *Astrophys. J.* **594** 1 (2003) [astro-ph/0305008]
- [36] S. Perlmutter et al., *Astrophys. J.* **517** 565 (1999) [astro-ph/9812133]
- [37] A.G. Riess et al., *Astron. J.* **117**, 707 (1999)
- [38] S. Jha, Ph.D. thesis, Harvard University (2002)

- [39] K. Krisciunas, *Astron. J.* **122**, 1616 (2001) [astro-ph/0106313]
- [40] A.G. Riess et al., *Astrophys. J.* **607**, 665 (2004) [astro-ph/0402512]
- [41] <http://astro.berkeley.edu/~saurabh/mlcs2k2/>
- [42] S.W. Allen, et al., *Mon. Not. Roy. Astron. Soc.* **353**, 457 (2004) [astro-ph/0405340]
- [43] R. G. Abraham et al [GDDS Collaboration] *Astron. J.* **593**, 622 (2003)
- [44] T. Treu et al., *Mon. Not. Roy. Astron. Soc.* **308** 1037 (1999)
- [45] T. Treu et al *Mon. Not. Roy. Astron. Soc.* **326** 221 (2001)
- [46] Y.G Gong, A.Z Wang, *Phys. Rev. D* **73**, 083506 (2006) [astro-ph/0601453]
- [47] Y.G Gong, A.Z Wang, *Phys. Rev. D* **75**, 043520 (2007) [astro-ph/0612196]
- [48] J.M. Virey et al., *Phys. Rev. D* **72**, 061302 (2005)
- [49] M.S. Turner, A.G. Riess et al., *Astrophys. J.* **569**, 18 (2002)
- [50] C.A. Shapiro, M.S. Turner, astro-ph/0512586.
- [51] W.L. Freedman et al., *Astrophys. J.* **553**, 47 (2001) [astro-ph/0012376]
- [52] R.A. Daly, S.G. Djorgovski, [arXiv:0710.5690]
- [53] R.A. Daly, S.G. Djorgovski, *Astrophys. J.*, **597**, 9 (2003)
- [54] R.A. Daly, S.G. Djorgovski, *Astrophys. J.*, **612**, 652 (2004)
- [55] J. Simon et al *Phys. Rev. D* **71**, 123001 (2005)
- [56] J.R. Bond, G. Efstathiou, M. Tegmark, *Mon. Not. Roy. Astron. Soc.* **291**, L33 (1997) [astro-ph/9702100]
- [57] D.J. Eisenstein, W. Hu, *Astrophys. J.* **496**, 605 (1998) [astro-ph/9709112]
- [58] U. Alam, V. Sahni, *Phys. Rev. D* **73**, 084024(2006) [astro-ph/0511473]
- [59] M. Arnaud, [astro-ph/0508159]
- [60] S. Nesseris, L. Perivolaropoulos, *J. Cosmol. Astron. Phys.* **0701**, 018 (2007) [astro-ph/0610092]
- [61] F.Y. Wang, *J. Cosmol. Astron. Phys.* **0803**, 020 (2007)
- [62] M. Biesiada, *J. Cosmol. Astron. Phys.* **0702** 003 (2007), astro-ph/0701721
- [63] A.R. Liddle, *Mon. Not. R. Astron. Soc.* **351** L49 (2004), astro-ph/0401198
- [64] D. Parkinson, S. Tsujikawa, B.A. Bassett, L. Amendola, *Phys. Rev. D* **71**, 063524, (2005)
- [65] W. Godlowski, M. Szydlowski, *Phys. Lett. B* **623** 10 (2005), astro-ph/0507322
- [66] M. Szydlowski, W. Godlowski, *Phys. Lett. B* **633** 427 (2006), astro-ph/0509415
- [67] L.X. Xu, C.W. Zhang, H.Y. Liu, *Chin. Phys. Lett.* **24** 2459 (2007).
- [68] M. Szydlowski, A. Kurek, A. Krawiec, *Phys. Lett. B* **642** 171 (2006), astro-ph/0604327

5. Appendix

TABLE IV: The two sets of SNe Ia data with their subsets.

192 ESSENCE SNe Ia data						182 Gold SNe Ia data				
Number	SN	z	μ	σ_μ	Subsample	SN	z	μ	σ_μ	Subsample
1	b013	0.4260	41.98	0.23	ESSENCE	SN95K	0.478	42.48	0.23	HZSST
2	d033	0.5310	42.96	0.17	ESSENCE	SN96E	0.425	41.69	0.40	HZSST
3	d083	0.3330	40.71	0.14	ESSENCE	SN96H	0.620	43.11	0.28	HZSST
4	d084	0.5190	42.95	0.29	ESSENCE	SN96I	0.570	42.80	0.25	HZSST
5	d085	0.4010	41.96	0.22	ESSENCE	SN96J	0.300	41.01	0.25	HZSST
6	d086	0.2050	40.08	0.30	ESSENCE	SN96K	0.380	42.02	0.22	HZSST
7	d089	0.4360	42.05	0.20	ESSENCE	SN96U	0.430	42.33	0.34	HZSST
8	d093	0.3630	41.73	0.14	ESSENCE	SN97as	0.508	42.19	0.35	HZSST
9	d097	0.4360	42.10	0.17	ESSENCE	SN97bb	0.518	42.83	0.31	HZSST
10	d117	0.3090	41.42	0.27	ESSENCE	SN97bj	0.334	40.92	0.30	HZSST
11	d149	0.3420	41.63	0.21	ESSENCE	SN97ce	0.440	42.07	0.19	HZSST
12	e020	0.1590	39.79	0.29	ESSENCE	SN97cj	0.500	42.73	0.20	HZSST
13	e029	0.3320	41.51	0.28	ESSENCE	SN98ac	0.460	41.81	0.40	HZSST
14	e108	0.4690	42.28	0.16	ESSENCE	SN98M	0.630	43.26	0.37	HZSST
15	e132	0.2390	40.42	0.29	ESSENCE	SN98J	0.828	43.59	0.61	HZSST
16	e136	0.3520	41.62	0.27	ESSENCE	SN99Q2*	0.459	42.67	0.22	HZSST
17	e138	0.6120	42.99	0.18	ESSENCE	SN99U2	0.511	42.83	0.21	HZSST
18	e140	0.6310	42.89	0.18	ESSENCE	SN99S*	0.474	42.81	0.22	HZSST
19	e147	0.6450	43.01	0.18	ESSENCE	SN99N	0.537	42.85	0.41	HZSST
20	e148	0.4290	42.25	0.20	ESSENCE	SN99fn	0.477	42.38	0.21	HZSST
21	e149	0.4970	42.23	0.26	ESSENCE	SN99ff	0.455	42.29	0.28	HZSST
22	f011	0.5390	42.66	0.25	ESSENCE	SN99fj	0.815	43.75	0.33	HZSST
23	f041	0.5610	42.72	0.17	ESSENCE	SN99fm	0.949	44.00	0.24	HZSST
24	f231	0.6190	43.05	0.17	ESSENCE	SN99fk	1.056	44.35	0.23	HZSST
25	f235	0.4220	41.78	0.24	ESSENCE	SN99fw	0.278	41.01	0.41	HZSST
26	f244	0.5400	42.72	0.26	ESSENCE	SN99fv*	1.199	44.19	0.34	HZSST
27	g005	0.2180	40.37	0.26	ESSENCE	SN00ec*	0.470	42.76	0.21	HZSST
28	g050	0.6330	42.77	0.18	ESSENCE	SN00dz	0.500	42.74	0.24	HZSST
29	g052	0.3830	41.56	0.22	ESSENCE	SN00eg	0.540	41.96	0.41	HZSST
30	g055	0.3020	41.39	0.37	ESSENCE	SN00ee*	0.470	42.73	0.23	HZSST
31	g097	0.3400	41.56	0.31	ESSENCE	SN00eh	0.490	42.40	0.25	HZSST
32	g120	0.5100	42.30	0.21	ESSENCE	SN01jh	0.884	44.22	0.19	HZSST
33	g133	0.4210	42.22	0.33	ESSENCE	SN01hu	0.882	43.89	0.30	HZSST
34	g142	0.3990	41.96	0.43	ESSENCE	SN01iy	0.570	42.87	0.31	HZSST
35	g160	0.4930	42.38	0.26	ESSENCE	SN01jp	0.528	42.76	0.25	HZSST
36	g240	0.6870	43.04	0.20	ESSENCE	SN01fo*	0.771	43.12	0.17	HZSST
37	h283	0.5020	42.49	0.37	ESSENCE	SN01hs	0.832	43.55	0.29	HZSST
38	h300	0.6870	43.09	0.17	ESSENCE	SN01hx	0.798	43.88	0.31	HZSST
39	h319	0.4950	42.40	0.21	ESSENCE	SN01hy	0.811	43.97	0.35	HZSST
40	h323	0.6030	43.01	0.22	ESSENCE	SN01jf	0.815	44.09	0.28	HZSST

TABLE IV continued

192 ESSENCE SNe Ia data						182 Gold SNe Ia data				
Number	SN	z	μ	σ_μ	Subsample	SN	z	μ	σ_μ	Subsample
41	h342	0.4210	42.18	0.16	ESSENCE	SN01jm	0.977	43.91	0.26	HZSST
42	h359	0.3480	41.89	0.27	ESSENCE	SN95aw	0.400	42.04	0.19	SCP
43	h363	0.2130	40.33	0.33	ESSENCE	SN95ax	0.615	42.85	0.23	SCP
44	h364	0.3440	41.32	0.17	ESSENCE	SN95ay	0.480	42.37	0.20	SCP
45	k425	0.2740	41.12	0.28	ESSENCE	SN95az	0.450	42.13	0.21	SCP
46	k429	0.1810	39.89	0.17	ESSENCE	SN95ba	0.388	42.07	0.19	SCP
47	k448	0.4010	42.34	0.40	ESSENCE	SN96ci	0.495	42.25	0.19	SCP
48	k485	0.4160	42.16	0.39	ESSENCE	SN96cl	0.828	43.96	0.46	SCP
49	m027	0.2860	41.53	0.32	ESSENCE	SN97eq	0.538	42.66	0.18	SCP
50	m158	0.4630	42.58	0.28	ESSENCE	SN97ek	0.860	44.03	0.30	SCP
51	m193	0.3410	41.29	0.23	ESSENCE	SN97ez	0.778	43.81	0.35	SCP
52	n256	0.6310	43.09	0.15	ESSENCE	SN97F	0.580	43.04	0.21	SCP
53	n263	0.3680	41.56	0.17	ESSENCE	SN97H	0.526	42.56	0.18	SCP
54	n278	0.3090	41.16	0.21	ESSENCE	SN97I	0.172	39.79	0.18	SCP
55	n285	0.5280	42.63	0.26	ESSENCE	SN97N	0.180	39.98	0.18	SCP
56	n326	0.2680	40.81	0.26	ESSENCE	SN97P	0.472	42.46	0.19	SCP
57	n404	0.2160	40.59	0.31	ESSENCE	SN97Q	0.430	41.99	0.18	SCP
58	p454	0.6950	43.53	0.17	ESSENCE	SN97R	0.657	43.27	0.20	SCP
59	p455	0.2840	41.10	0.29	ESSENCE	SN97ac	0.320	41.45	0.18	SCP
60	p524	0.5080	42.43	0.22	ESSENCE	SN97af	0.579	42.86	0.19	SCP
61	SN92ag	0.0259	35.14	0.22	nearby	SN97ai	0.450	42.10	0.23	SCP
62	SN92bc	0.0198	34.84	0.18	nearby	SN97aj	0.581	42.63	0.19	SCP
63	SN92bo	0.0181	34.73	0.21	nearby	SN97am	0.416	42.10	0.19	SCP
64	SN94S	0.0160	34.35	0.22	nearby	SN97ap	0.830	43.85	0.19	SCP
65	SN95ak	0.0220	34.70	0.21	nearby	SN98ba	0.430	42.36	0.25	SCP
66	SN96bo	0.0163	33.98	0.24	nearby	SN98bi	0.740	43.35	0.30	SCP
67	SN97Y	0.0166	34.53	0.23	nearby	SN00fr	0.543	42.67	0.19	SCP
68	SN98V	0.0172	34.36	0.22	nearby	SN90T	0.040	36.38	0.20	LR
69	SN98ab	0.0279	35.17	0.18	nearby	SN91U	0.033	35.53	0.21	LR
70	SN98ef	0.0167	34.16	0.23	nearby	SN91S	0.056	37.31	0.19	LR
71	SN98eg	0.0235	35.32	0.20	nearby	SN92bg	0.036	36.17	0.20	LR
72	SN99aw	0.0392	36.54	0.13	nearby	SN92bk	0.058	37.13	0.19	LR
73	SN99ek	0.0176	34.28	0.22	nearby	SN92J	0.046	36.35	0.21	LR
74	SN00ca	0.0245	35.24	0.17	nearby	SN92au	0.061	37.31	0.22	LR
75	SN00cn	0.0232	35.12	0.18	nearby	SN93ah	0.028	35.53	0.22	LR
76	SN00dk	0.0164	34.37	0.22	nearby	SN94Q	0.029	35.70	0.21	LR
77	SN00fa	0.0218	34.90	0.21	nearby	SN98cs	0.032	36.08	0.20	LR
78	SN01V	0.0162	34.14	0.22	nearby	SN99ef	0.038	36.67	0.19	LR
79	SN01ba	0.0305	35.88	0.16	nearby	SN99X	0.025	35.40	0.22	LR
80	SN01cz	0.0163	34.28	0.24	nearby	SN00bk	0.026	35.35	0.23	LR

TABLE IV continued

192 ESSENCE SNe Ia data						182 Gold SNe Ia data				
Number	SN	z	μ	σ_μ	Subsample	SN	z	μ	σ_μ	Subsample
81	SN90O	0.0306	35.81	0.17	nearby	SN90O	0.030	35.90	0.21	LR
82	SN90af	0.0502	36.69	0.20	nearby	SN90af	0.050	36.84	0.22	LR
83	SN92P	0.0263	35.60	0.19	nearby	SN92P	0.026	35.63	0.22	LR
84	SN92ae	0.0748	37.72	0.21	nearby	SN92ae	0.075	37.77	0.19	LR
85	SN92aq	0.1009	38.80	0.15	nearby	SN92aq	0.101	38.70	0.20	LR
86	SN92bh	0.0451	36.91	0.19	nearby	SN92bh	0.045	36.99	0.18	LR
87	SN92bl	0.0429	36.49	0.18	nearby	SN92bl	0.043	36.52	0.19	LR
88	SN92bp	0.0789	37.78	0.15	nearby	SN92bp	0.079	37.94	0.18	LR
89	SN92br	0.0878	37.76	0.23	nearby	SN92br	0.088	38.07	0.28	LR
90	SN92bs	0.0634	37.64	0.20	nearby	SN92bs	0.063	37.67	0.19	LR
91	SN93B	0.0707	37.78	0.19	nearby	SN93B	0.071	37.78	0.19	LR
92	SN93H	0.0248	35.10	0.18	nearby	SN93H	0.025	35.09	0.22	LR
93	SN93O	0.0519	37.12	0.15	nearby	SN93O	0.052	37.16	0.18	LR
94	SN93ag	0.0500	37.07	0.18	nearby	SN93ag	0.050	37.07	0.19	LR
95	SN94M	0.0243	35.24	0.20	nearby	SN94M	0.024	35.09	0.22	LR
96	SN94T	0.0357	36.02	0.17	nearby	SN94T	0.036	36.01	0.21	LR
97	SN95ac	0.0488	36.57	0.16	nearby	SN95ac	0.049	36.55	0.20	LR
98	SN96C	0.0275	35.94	0.18	nearby	SN96C	0.027	35.90	0.21	LR
99	SN96ab	0.1242	38.90	0.20	nearby	SN96ab	0.124	39.19	0.22	LR
100	SN96bl	0.0348	36.09	0.18	nearby	SN96bl	0.034	36.19	0.20	LR
101	SN97dg	0.0297	36.15	0.19	nearby	SN97dg	0.029	36.13	0.21	LR
102	SN98dx	0.0537	36.92	0.15	nearby	SN98dx	0.053	36.95	0.19	LR
103	SN99cc	0.0315	35.82	0.17	nearby	SN99cc	0.031	35.84	0.21	LR
104	SN99gp	0.0260	35.62	0.16	nearby	SN99gp	0.026	35.57	0.21	LR
105	SN00cf	0.0365	36.36	0.17	nearby	SN00cf	0.036	36.39	0.19	LR
106	1977ff	1.7550	45.31	0.36	HST	1997ff	1.755	45.35	0.35	HST
107	2002dc	0.4750	42.20	0.21	HST	2002dc	0.475	42.24	0.20	HST
108	2002dd	0.9500	43.94	0.35	HST	2002dd	0.950	43.98	0.34	HST
109	2003eq	0.8400	43.63	0.22	HST	2003eq	0.840	43.67	0.21	HST
110	2003es	0.9540	44.26	0.28	HST	2003es	0.954	44.30	0.27	HST
111	2003eb	0.9000	43.60	0.26	HST	2003eb	0.900	43.64	0.25	HST
112	2003XX	0.9350	43.93	0.30	HST	2003XX	0.935	43.97	0.29	HST
113	2003bd	0.6700	43.15	0.25	HST	2003bd	0.670	43.19	0.24	HST
114	2002kd	0.7350	43.10	0.20	HST	2002kd	0.735	43.14	0.19	HST
115	2003be	0.6400	42.97	0.26	HST	2003be	0.640	43.01	0.25	HST
116	2003dy	1.3400	44.88	0.32	HST	2003dy	1.340	44.92	0.31	HST
117	2002ki	1.1400	44.67	0.30	HST	2002ki	1.140	44.71	0.29	HST
118	2002hp	1.3050	44.47	0.31	HST	2002hp	1.305	44.51	0.30	HST
119	2002fw	1.3000	45.02	0.21	HST	2002fw	1.300	45.06	0.20	HST
120	HST04Pat	0.9700	44.63	0.37	HST	HST04Pat	0.970	44.67	0.36	HST

TABLE IV continued

192 ESSENCE SNe Ia data						182 Gold SNe Ia data				
Number	SN	z	μ	σ_μ	Subsample	SN	z	μ	σ_μ	Subsample
121	HST04Mcg	1.3700	45.19	0.26	HST	HST04Mcg	1.370	45.23	0.25	HST
122	HST05Fer	1.0200	43.95	0.28	HST	HST05Fer	1.020	43.99	0.27	HST
123	HST05Koe	1.2300	45.13	0.24	HST	HST05Koe	1.230	45.17	0.23	HST
124	HST04Gre	1.1400	44.40	0.32	HST	HST04Gre	1.140	44.44	0.31	HST
125	HST04Omb	0.9750	44.17	0.27	HST	HST04Omb	0.975	44.21	0.26	HST
126	HST05Lan	1.2300	44.93	0.21	HST	HST05Lan	1.230	44.97	0.20	HST
127	HST04Tha	0.9540	43.81	0.28	HST	HST04Tha	0.954	43.85	0.27	HST
128	HST04Rak	0.7400	43.34	0.23	HST	HST04Rak	0.740	43.38	0.22	HST
129	HST04Yow	0.4600	42.19	0.33	HST	HST04Yow	0.460	42.23	0.32	HST
130	HST04Man	0.8540	43.92	0.30	HST	HST04Man	0.854	43.96	0.29	HST
131	HST05Spo	0.8390	43.41	0.21	HST	HST05Spo	0.839	43.45	0.20	HST
132	HST04Eag	1.0200	44.48	0.20	HST	HST04Eag	1.020	44.52	0.19	HST
133	HST05Gab	1.1200	44.63	0.19	HST	HST05Gab	1.120	44.67	0.18	HST
134	HST05Str	1.0100	44.73	0.20	HST	HST05Str	1.010	44.77	0.19	HST
135	HST04Sas	1.3900	44.86	0.20	HST	HST04Sas	1.390	44.90	0.19	HST
136	SN03D1au	0.5043	42.55	0.18	SNLS	SN03D1au	0.504	42.61	0.17	SNLS
137	SN03D1aw	0.5817	43.12	0.21	SNLS	SN03D1aw	0.582	43.07	0.17	SNLS
138	SN03D1ax	0.4960	42.33	0.20	SNLS	SN03D1ax	0.496	42.36	0.17	SNLS
139	SN03D1co	0.6790	43.59	0.27	SNLS	SN03D1co	0.679	43.58	0.19	SNLS
140	SN03D1fc	0.3310	41.30	0.21	SNLS	SN03D1fc	0.331	41.13	0.17	SNLS
141	SN03D1fl	0.6880	43.13	0.23	SNLS	SN03D1fl	0.688	43.23	0.17	SNLS
142	SN03D1fq	0.8000	43.92	0.27	SNLS	SN03D1fq	0.800	43.67	0.19	SNLS
143	SN03D3af	0.5320	42.84	0.29	SNLS	SN03D3af	0.532	42.78	0.18	SNLS
144	SN03D3aw	0.4490	42.07	0.24	SNLS	SN03D3aw	0.449	42.05	0.17	SNLS
145	SN03D3ay	0.3709	41.80	0.23	SNLS	SN03D3ay	0.371	41.67	0.17	SNLS
146	SN03D3cc	0.4627	42.25	0.17	SNLS	SN03D3cc	0.463	42.27	0.17	SNLS
147	SN03D3cd	0.4607	42.12	0.18	SNLS	SN03D3cd	0.461	42.22	0.17	SNLS
148	SN03D4ag	0.2850	40.98	0.13	SNLS	SN03D4ag	0.285	40.92	0.17	SNLS
149	SN03D4at	0.6330	43.26	0.25	SNLS	SN03D4at	0.633	43.32	0.18	SNLS
150	SN03D4cx	0.9490	44.26	0.17	SNLS	SN03D4cx	0.949	43.69	0.32	SNLS
151	SN03D4cz	0.6950	43.11	0.34	SNLS	SN03D4cz	0.695	43.21	0.19	SNLS
152	SN03D4dh	0.6268	42.94	0.23	SNLS	SN03D4dh	0.627	42.93	0.17	SNLS
153	SN03D4di	0.9050	43.84	0.16	SNLS	SN03D4di	0.905	43.89	0.30	SNLS
154	SN03D4dy	0.6040	42.79	0.32	SNLS	SN03D4dy	0.604	42.70	0.17	SNLS
155	SN03D4fd	0.7910	43.75	0.21	SNLS	SN03D4fd	0.791	43.54	0.18	SNLS
156	SN03D4gg	0.5920	42.87	0.25	SNLS	SN03D4gg	0.592	42.75	0.19	SNLS
157	SN04D2fp	0.4150	42.06	0.17	SNLS	SN04D2fp	0.415	41.96	0.17	SNLS
158	SN04D2fs	0.3570	41.65	0.22	SNLS	SN04D2fs	0.357	41.63	0.17	SNLS
159	SN04D2gb	0.4300	41.81	0.18	SNLS	SN04D2gb	0.430	41.96	0.17	SNLS
160	SN04D3co	0.6200	43.20	0.26	SNLS	SN04D3co	0.620	43.21	0.18	SNLS

TABLE IV continued

192 ESSENCE SNe Ia data						182 Gold SNe Ia data				
Number	SN	z	μ	σ_μ	Subsample	SN	z	μ	σ_μ	Subsample
161	SN04D3cy	0.6430	43.34	0.22	SNLS	SN04D3cy	0.643	43.21	0.18	SNLS
162	SN04D3df	0.4700	42.03	0.20	SNLS	SN04D3df	0.470	42.45	0.17	SNLS
163	SN04D3do	0.6100	42.82	0.29	SNLS	SN04D3do	0.610	42.98	0.17	SNLS
164	SN04D3ez	0.2630	40.76	0.21	SNLS	SN04D3ez	0.263	40.87	0.17	SNLS
165	SN04D3fk	0.3578	41.41	0.21	SNLS	SN04D3fk	0.358	41.66	0.17	SNLS
166	SN04D3fq	0.7300	43.57	0.26	SNLS	SN04D3fq	0.730	43.47	0.18	SNLS
167	SN04D3hn	0.5516	42.28	0.41	SNLS	SN04D3hn	0.552	42.65	0.17	SNLS
168	SN04D3kr	0.3373	41.46	0.17	SNLS	SN04D3kr	0.337	41.44	0.17	SNLS
169	SN04D3lu	0.8218	43.76	0.22	SNLS	SN04D3lu	0.822	43.73	0.27	SNLS
170	SN04D3ml	0.9500	44.14	0.15	SNLS	SN04D3ml	0.950	44.14	0.31	SNLS
171	SN04D3nh	0.3402	41.63	0.17	SNLS	SN04D3nh	0.340	41.51	0.17	SNLS
172	SN04D4an	0.6130	43.08	0.39	SNLS	SN04D4an	0.613	43.15	0.18	SNLS
173	SN04D4bq	0.5500	42.75	0.29	SNLS	SN04D4bq	0.550	42.67	0.17	SNLS
174	SN03D1bp	0.3460	41.50	0.25	SNLS	SN03D1cm	0.870	44.28	0.34	SNLS
175	SN03D1ew	0.8680	43.95	0.17	SNLS	SN03D3bh	0.249	40.76	0.17	SNLS
176	SN03D3ba	0.2912	40.56	0.32	SNLS	SN03D4gl	0.571	42.65	0.18	SNLS
177	SN03D4cn	0.8180	44.14	0.27	SNLS	SN04D1ag	0.557	42.70	0.17	SNLS
178	SN03D4gf	0.5810	42.85	0.18	SNLS	SN04D2cf	0.369	41.67	0.17	SNLS
179	SN04D1aj	0.7210	43.46	0.23	SNLS	SN04D2gp	0.707	43.42	0.21	SNLS
180	SN04D1ak	0.5260	42.49	0.29	SNLS	SN04D3oe	0.756	43.64	0.17	SNLS
181	SN04D2gc	0.5210	42.44	0.33	SNLS	SN04D4dm	0.811	44.13	0.31	SNLS
182	SN04D2iu	0.6910	43.42	0.39	SNLS	SN04D4dw	0.961	44.18	0.33	SNLS
183	SN04D2ja	0.7410	43.58	0.24	SNLS					
184	SN04D3cp	0.8300	43.62	0.17	SNLS					
185	SN04D3dd	1.0100	44.70	0.17	SNLS					
186	SN04D3gt	0.4510	41.35	0.23	SNLS					
187	SN04D3gx	0.9100	44.21	0.18	SNLS					
188	SN04D3is	0.7100	43.71	0.34	SNLS					
189	SN04D3ki	0.9300	44.43	0.19	SNLS					
190	SN04D3ks	0.7520	43.36	0.23	SNLS					
191	SN04D3nc	0.8170	43.72	0.21	SNLS					
192	SN04D4bk	0.8400	43.88	0.17	SNLS					

Note.— In the TABLE IV, * denotes the six outliers of the HZSST subset.